Evaporative cooling over the Tibetan Plateau induced by vegetation growth

Miaogen Shen[a,b,1], Shilong Piao[a,b,c,1], Su-Jong Jeong[d], Liming Zhou[e], Zhenzhong Zeng[c], Philippe Ciais[f], Deliang Chen[g], Mengtian Huang[c], Chun-Sil Jin[h], Laurent Z. X. Li[i], Yue Li[c], Ranga B. Myneni[j], Kun Yang[a,b], Gengxin Zhang[a], Yangjian Zhang[b,k], and Tandong Yao[a,b]

[a]Institute of Tibetan Plateau Research, Chinese Academy of Sciences, Beijing 100101, China; [b]Chinese Academy of Sciences Center for Excellence in Tibetan Plateau Earth Sciences, Chinese Academy of Sciences, Beijing 100101, China; [c]Department of Ecology, College of Urban and Environmental Sciences, Peking University, Beijing 100871, China; [d]Jet Propulsion Laboratory, California Institute of Technology, Pasadena, CA 91011; [e]Department of Atmospheric and Environmental Sciences, University at Albany, State University of New York, Albany, NY 12222; [f]Laboratoire des Sciences du Climat et de l'Environnement, UMR 1572 Commissariat à l'Energie Atomique-CNRS, Université de Versailles St-Quentin-en-Yvelines, 91191 Gif-sur-Yvette, France; [g]Department of Earth Sciences, University of Gothenberg, 405 30 Gothenberg, Sweden; [h]School of Earth and Environmental Sciences, Seoul National University, Seoul 151-747, Korea; [i]Laboratoire de Météorologie Dynamique, CNRS, Université Pierre et Marie Curie-Paris 6, 75252 Paris, France; [j]Department of Earth and Environment, Boston University, Boston, MA 02215; and [k]Key Laboratory of Ecosystem Network Observation and Modeling, Institute of Geographic Sciences and Natural Resources Research, Chinese Academy of Sciences, Beijing 100101, China

Edited by Roni Avissar, University of Miami, Miami, FL, and accepted by the Editorial Board June 11, 2015 (received for review March 4, 2015)

In the Arctic, climate warming enhances vegetation activity by extending the length of the growing season and intensifying maximum rates of productivity. In turn, increased vegetation productivity reduces albedo, which causes a positive feedback on temperature. Over the Tibetan Plateau (TP), regional vegetation greening has also been observed in response to recent warming. Here, we show that in contrast to arctic regions, increased growing season vegetation activity over the TP may have attenuated surface warming. This negative feedback on growing season vegetation temperature is attributed to enhanced evapotranspiration (ET). The extra energy available at the surface, which results from lower albedo, is efficiently dissipated by evaporative cooling. The net effect is a decrease in daily maximum temperature and the diurnal temperature range, which is supported by statistical analyses of in situ observations and by decomposition of the surface energy budget. A daytime cooling effect from increased vegetation activity is also modeled from a set of regional weather research and forecasting (WRF) mesoscale model simulations, but with a magnitude smaller than observed, likely because the WRF model simulates a weaker ET enhancement. Our results suggest that actions to restore native grasslands in degraded areas, roughly one-third of the plateau, will both facilitate a sustainable ecological development in this region and have local climate cobenefits. More accurate simulations of the biophysical coupling between the land surface and the atmosphere are needed to help understand regional climate change over the TP, and possible larger scale feedbacks between climate in the TP and the Asian monsoon system.

climate change | feedback | evapotranspiration | vegetation | Tibetan Plateau

The Tibetan Plateau (TP) plays a key role in the Asian summer monsoon, a weather system affecting more than half of the world's population. The TP has experienced a pronounced warming over recent decades (1), with a warming rate of about twice the global average for the period 1960–2009 (2, 3), yet with heterogeneous patterns. Both observations and model studies show that recent climate change has had an impact on the structure and ecological functioning of TP grasslands (4–7). One robust observation is that temperature has increased more slowly during the day than during the night, thereby reducing the diurnal temperature range by about 0.23 °C per decade over the period 1961–2003 (8). Understanding the mechanisms driving the spatiotemporal patterns of temperature change over the TP is critical for the development of adaptation strategies to protect its vulnerable grassland ecosystems and for better understanding the coupling between regional changes over the TP and the larger Asian monsoon system (9).

Changes in vegetation albedo, emissivity, and evapotranspiration (ET) altogether exert feedbacks on climate (10–14). In the Arctic, it has been shown that a temperature-driven increase of vegetation productivity can produce a positive feedback to warming through reduced albedo, which increases the amount of solar radiation absorbed by the surface (11, 14, 15). However, such a positive albedo feedback may be partially offset by increased cooling from higher ET (16–18). The balance between these two biophysical mechanisms of opposite sign in the surface energy budget likely determines how vegetation changes affect local climate, but little observational evidence exists to demonstrate vegetation feedbacks on climate at regional or continental scales (19, 20). For the TP, it is as yet unknown whether the vegetation changes may have contributed to local temperature variations. The goal of this study is to investigate how changes in vegetation greenness exert influences on local temperature. To that end, we have used satellite-measured vegetation greenness, the Normalized Difference Vegetation Index (NDVI), as a proxy of vegetation activity (photosynthesis and vegetation coverage), in combination with in situ air temperature observations and three independent gridded ET estimates, one based on the Penman–Monteith equation and Moderate-resolution Imaging

Significance

Understanding land-surface biophysical feedbacks to the atmosphere is needed if we are to simulate regional climate accurately. In the Arctic, previous studies have shown that enhanced vegetation growth decreases albedo and amplifies warming. In contrast, on the Tibetan Plateau, a statistical model based on in situ observations and decomposition of the surface energy budget suggests that increased vegetation activity may attenuate daytime warming by enhancing evapotranspiration (ET), a cooling process. A regional climate model also simulates daytime cooling when prescribed with increased vegetation activity, but with a magnitude smaller than observed, likely because this model simulates weaker ET enhancement in response to increased vegetation growth.

Author contributions: S.P. designed research; M.S. performed research; S.-J.J., C.-S.J., and L.Z.X.L. contributed new reagents/analytic tools; M.S. and Z.Z. analyzed data; and M.S., S.P., L.Z., P.C., D.C., M.H., L.Z.X.L., Y.L., R.B.M., K.Y., G.Z., Y.Z., and T.Y. wrote the paper.

The authors declare no conflict of interest.

This article is a PNAS Direct Submission. R.A. is a guest editor invited by the Editorial Board.

[1]To whom correspondence may be addressed. Email: shen.miaogen@gmail.com or slpiao@pku.edu.cn.

This article contains supporting information online at www.pnas.org/lookup/suppl/doi:10.1073/pnas.1504418112/-/DCSupplemental.

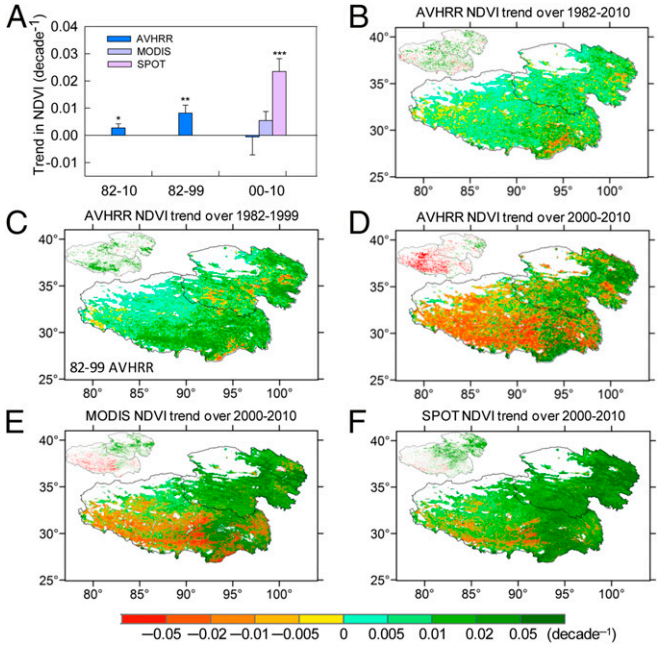

Fig. 1. Changes in the growing season (May–September) NDVI across the TP over the past three decades. (*A*) Trend in the growing season NDVI at a regional scale over 1982–2010, 1982–1999, and 2000–2010. The pixels with growing season NDVI lower than 0.10 are not considered. ***$P < 0.01$; **$P < 0.05$; *$P < 0.10$. Trends with no asterisk are not significant ($P > 0.10$). (*B–F*) Spatial distribution of the growing season NDVI trend for the different datasets and periods. (*Insets*) Pixels with significantly ($P < 0.05$) negative (red) or positive (green) trends are shown in each map.

Spectroradiometer (MODIS) land products (ET_M), the second based on the Priestley and Taylor equation [Global Land Surface Evaporation: the Amsterdam Methodology (GLEAM); ET_G], and the third from a machine-learning algorithm that interpolates flux-tower ET measurements in time and space (ET_J). A sensitivity analysis of the ET cooling effect based on intrinsic biophysical mechanisms and simulations from the Weather Research and Forecasting (WRF) regional climate model (*Methods*) are used as well.

Results

Relationships Between Greening and Temperature Trends. We first characterize changes in the growing season (May to September) NDVI using three different satellite-derived NDVI datasets: one from an Advanced Very High Resolution Radiometer (AVHRR; 1982–2010) and two others from a MODIS (2000–2010) and Système Pour l'Observation de la Terre (SPOT)-VEGETATION (2000–2010) (*Methods*). The AVHRR NDVI data show a positive trend (i.e., greening) during the entire period 1982–2010 (Fig. 1 *A* and *B*). Consistent with an earlier study (21), the greening trend of the AVHRR NDVI over the TP mainly occurred during the 1980s and 1990s (Fig. 1 *A* and *C*). During their period of overlap in the 2000s, the three NDVI datasets (Fig. 1*A*) exhibit similar spatial patterns of the trends (Fig. 1 *D–F*) but different mean trends when averaged over the entire TP area (Fig. 1*A*). All three datasets show a systematic decrease in the growing season NDVI over the past decade in the southwest of the plateau. This decrease is associated with a delayed vegetation green-up date (22). In contrast, greening persisted over the northeast of the TP.

We hypothesize that through mechanisms of land surface feedback, spatial differences in temporal trend of the NDVI ($NDVI_{trend}$) across the TP region (Fig. 1 *B–F*) affect regional patterns of surface temperature trend. To test this hypothesis, we first investigated the spatial relationship between observed $NDVI_{trend}$ and the temporal trend ($T_{mean,trend}$) of growing season average of daily mean temperature (T_{mean}) from 55 meteorological stations. Because vegetation growth over the TP is limited by low temperature (Fig. S1), in the absence of feedbacks, one would expect a positive spatial correlation between $T_{mean,trend}$ and $NDVI_{trend}$. However, when $NDVI_{trend}$ is regressed against the meteorological station $T_{mean,trend}$, it is found that the correlation is negative ($P < 0.01$). This relationship remains robust regardless of the choice of NDVI dataset (Fig. 2 *A–E*), suggesting that increasing vegetation activity may exert a negative forcing (cooling) on local temperature trends.

Because changes in vegetation activity have asymmetrical effects on the diurnal cycle of surface air temperature (13), we examine the statistical relationships between $NDVI_{trend}$ and $T_{max,trend}$ which is the trend in daytime maximum temperature (T_{max}) and $T_{min,trend}$ which is the trend in nighttime minimum temperature (T_{min}). $NDVI_{trend}$ is found to have a stronger negative spatial correlation with $T_{max,trend}$ rather than with $T_{min,trend}$ (Fig. 2 *F–O*). $NDVI_{trend}$ from MODIS and SPOT is not significantly (Fig. 2 *N* and *O*) correlated with $T_{min,trend}$ across the 55 meteorological stations. Further, $NDVI_{trend}$ does not show significantly negative correlations with $T_{min,trend}$ when the confounding effects of T_{max} are statistically removed (Fig. 2 *K–O*). In contrast, accounting for the confounding effect of T_{min} on T_{max} does not affect the significantly negative correlation between $NDVI_{trend}$ and $T_{max,trend}$ (Fig. 2 *F–J*), suggesting that increasing vegetation activity may exert a cooling effect on local temperature trends, primarily in the daytime.

The spatially negative correlation between $NDVI_{trend}$ and $T_{max,trend}$ across the TP is expected to be stronger in summer when vegetation is more active and radiation is more intense. We did find a stronger negative correlation between $T_{max,trend}$ and $NDVI_{trend}$ for summer (July and August) than for spring (May and June) or for fall (September) (Fig. S2). In contrast, $T_{min,trend}$ consistently shows no significantly negative correlation with $NDVI_{trend}$ for all cases. Because of this nonsymmetrical effect of greening on T_{max} and T_{min}, the trend in diurnal temperature range is negatively correlated with $NDVI_{trend}$ ($P < 0.01$; Fig. S3 *B–E*), except for the period 1982–2010, during which the correlation is only marginally significant ($P = 0.07$; Fig. S3*A*).

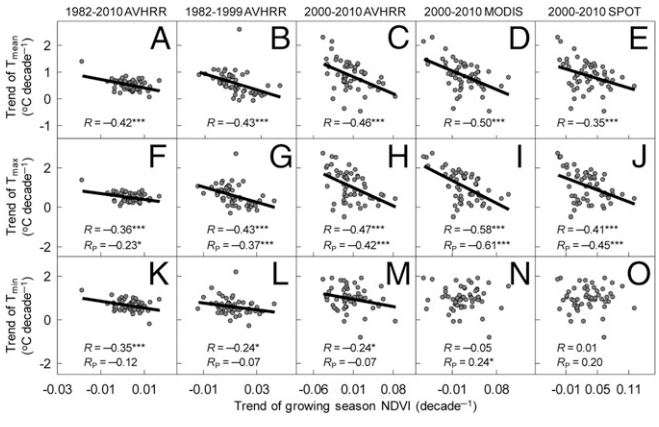

Fig. 2. Spatial relationship of the growing season NDVI trend with trend of T_{mean}, T_{max}, and T_{min} across the 55 meteorological stations in the TP. In each of the panels (*A–O*), the period for calculating the temporal trends and NDVI dataset are given in the top of the figure. Each point is for one station. *R* is the correlation coefficient between the trend of the growing season NDVI and the trend of temperature. R_P indicates partial correlation coefficients of the trend of the growing season NDVI with the trend of T_{max} (or T_{min}) through controlling T_{min} (or T_{max}). ***$P < 0.01$; *$P < 0.10$. Correlations with no asterisk are not significant ($P > 0.10$).

Possible Mechanisms. The significant negative correlation between $NDVI_{trend}$ and $T_{max,trend}$ suggests an ET-induced cooling effect in the daytime. ET is a key process that dissipates the energy absorbed by the vegetation and determines the diurnal cycle of near-surface air temperature. The cooling feedback due to increased ET in response to the positive trend of vegetation greenness is expected to reduce daytime (T_{max}) rather than nighttime (T_{min}) warming rates, and to have stronger impacts in the summer than in other seasons. This mechanism is consistent with evidence from the spatial patterns of observations. Next, we use statistical and numerical tools, as well as a sensitivity analysis, to investigate this mechanism further.

We first examine the spatial correlations between in situ $T_{max,trend}$ and the temporal trend in ET (ET_{trend}) from (*i*) ET_M products (MOD16A2-ET) for the period 2000–2010 (23), (*ii*) ET_G products over the period 2000–2010 (24), and (*iii*) ET_J products (25) over the period 1982–1999 (data descriptions are provided in *Methods*). For all three ET datasets, the spatial patterns of ET_{trend} are found to be negatively correlated with $T_{max,trend}$ ($P < 0.05$; Fig. 3*A*). In contrast, the patterns of $T_{min,trend}$ are not significantly correlated with ET_{trend} (from partial correlation, $P > 0.10$; Fig. 3*B*). In addition, the spatial pattern of ET_{trend} is significantly and positively correlated with $NDVI_{trend}$ for the three satellite NDVI datasets ($P < 0.10$ for GLEAM ET_{trend} and AVHRR $NDVI_{trend}$ and $P < 0.01$ for the other combinations of ET_{trend} and $NDVI_{trend}$; Fig. S4). Moreover, the negative correlations between $T_{max,trend}$ and ET_{trend} (or $NDVI_{trend}$) still hold when we statistically account for the trends of both T_{min} and albedo (or absorbed solar radiation) (Figs. S5 and S6). These results suggest that greening increases ET, which, in turn, cools T_{max}.

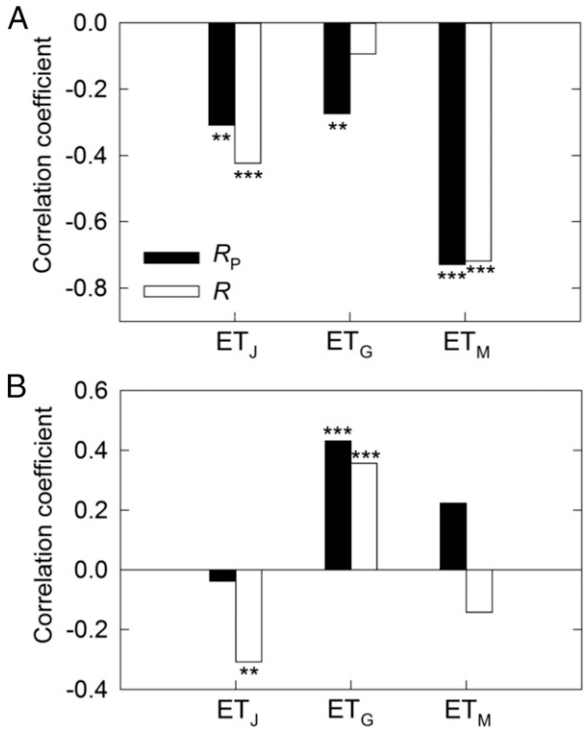

Fig. 3. Coefficient of the spatial correlation between growing season ET trend and T_{max} (*A*) and T_{min} (*B*) across the TP. *R* is the correlation coefficient. R_P is the partial correlation coefficient of the trend of growing season ET with the trend of T_{max} (or T_{min}) removing the effects of T_{min} (or T_{max}). ET was extracted from a dataset produced by a machine-learning algorithm using flux-tower measurements over 1982–1999 (ET_J) and ET_M (MOD16A2-ET) and ET_G products over 2000–2010. ***$P < 0.01$; **$P < 0.05$. Correlations with no asterisk are not significant ($P > 0.10$).

To quantify the effect of vegetation greenness on temperature, we perform a multiple linear regression analysis in which $T_{max,trend}$ is set as the dependent variable and $NDVI_{trend}$ and $T_{min,trend}$ are set as independent variables. This procedure can eliminate the influence from the relationship between $T_{max,trend}$ and $T_{min,trend}$, and it defines the linear regression slope of $NDVI_{trend}$ to $T_{max,trend}$ as the sensitivity of $T_{max,trend}$ to $NDVI_{trend}$. Different values of the regression slope are found for different decades and different satellite datasets, but the sign of the slopes always indicates a lower $T_{max,trend}$ where the NDVI has increased, which is consistent with the expectation that greening cools near-surface air temperature. These slopes range from -0.9 ± 0.5 °C to -1.3 ± 0.2 °C in response to an NDVI increase of 0.1 (Fig. S7*A*). Note that the NDVI is dimensionless and that an increase of 0.1 is comparable to the greatest $NDVI_{trend}$ in one decade, as shown in Fig. 2 *C*–*E*.

Next, we use the WRF, version 3.2 (WRF3.2) regional climate model (26) with the Noah land surface scheme (27) to simulate the magnitude of vegetation-to-temperature effects over the TP. Two simulations were performed: one without (S1) and one with (S2) prescribed day-to-day changes in growing season leaf area index (LAI) from AVHRR NDVI observations during the period 1982–2010 (*Methods*). The difference between S2 and S1 allows us to quantify the effect of greenness changes on surface air temperature. As shown in Fig. 4, the average S2−S1 difference of prescribed NDVI (ΔNDVI; used to define the LAI difference prescribed in WRF3.2) is spatially significantly ($P < 0.01$) and negatively correlated with the S2−S1 difference of modeled T_{max} (ΔT_{max}). Unlike the observation-based statistical analysis, which cannot separate forcing and feedbacks, the WRF simulations can quantify the feedbacks. The spatial correlation between ΔNDVI and simulated ΔT_{max} is stronger than the spatial correlation between ΔNDVI and the difference of modeled T_{min} (ΔT_{min}). Consistent with the observational analysis (Fig. S4), a significant and positive relationship is also found between ΔNDVI and the S2−S1 ET difference (ΔET), given by the Noah land surface model (27) in WRF3.2 ($P < 0.01$; Fig. S8*A*). In the WRF3.2 simulations, ΔET shows stronger spatial correlations with ΔT_{max} than with ΔT_{min} (Fig. S8 *B* and *C*), which supports the proposed mechanism of an evaporative cooling feedback whereby increased vegetation LAI reduces daytime air temperature over the TP region. However, the sensitivity of T_{max} to the prescribed LAI change (from the observed NDVI change) in WRF3.2 is much smaller than the sensitivity of T_{max} derived from the statistical analyses of long-term observations. The WRF3.2 simulations show that an increase in the NDVI by 0.1 results in a cooling of T_{max} by only 0.07 ± 0.01 °C ($P < 0.01$), which is merely 10% of the sensitivity of T_{max} to the NDVI diagnosed from observations (Fig. S7*A*).

To investigate why the model estimates of the biophysical cooling effect are smaller than observations, we examined whether the Noah land surface model of WRF3.2 realistically simulates changes in albedo. We first compared the modeled albedo with MODIS white sky albedo in the short-wave band (28). The simulated sensitivity of albedo to the NDVI (-0.09 ± 0.01) in WRF3.2 is close to the sensitivity of MODIS albedo to NDVI (-0.11 ± 0.01) as obtained from a spatial data regression analysis (Fig. S9). This comparison indicates that the smaller cooling effect in WRF3.2 could not be attributed to the model albedo biases. We then compared the sensitivity of ET to the NDVI in both WRF3.2 simulations and in the observations. Linear spatial regression between the S2−S1 ΔNDVI and the S2−S1 ΔET showed that a 0.1-unit increase in growing season NDVI is associated with an increase of ET by only 0.07 ± 0.01 mm·d^{-1} in WRF3.2 (Fig. S10). In contrast, the spatial ET sensitivity to the NDVI in the observations is 0.49 ± 0.13 mm·d^{-1}, and ranges from 0.20 ± 0.04 to 0.51 ± 0.10 mm·d^{-1} among different ET and NDVI datasets (Fig. S10). Therefore, the weaker ET cooling feedback likely results from the lower ET sensitivity to greenness

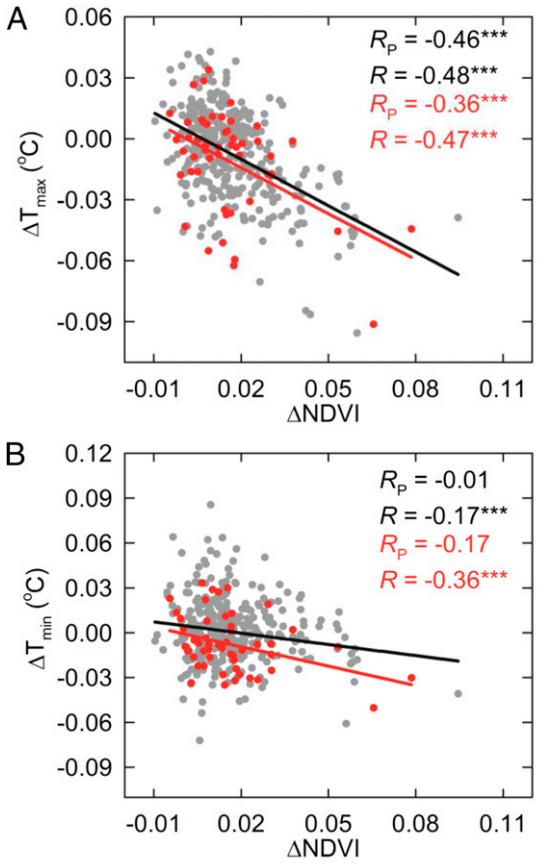

Fig. 4. Spatial statistical relationships between the temperature difference from two simulations of the WRF3.2-Noah regional climate model (S2−S1) and the growing season NDVI difference (ΔNDVI) prescribed in these simulations. In simulation S1, the LAI of the land surface model Noah is prescribed from the climatological NDVI. In simulation S2, the variable LAI from the observed LAI is prescribed. The difference between S2 and S1 gives the modeled effect of an increased NDVI on the regional climate daytime temperature difference (*A*; ΔT_{max}) and nighttime temperature difference (*B*; ΔT_{min}). ΔNDVI, ΔT_{max}, and ΔT_{min} are estimated as the differences in the 29-y averaged values of the growing season NDVI, T_{max}, and T_{min} between the S2 and S1 simulations, respectively. The red circles indicate the spatial correlations using the grids where meteorological stations are located and the gray and red ones altogether indicate all the grids. *R* is the correlation coefficient between the trend of the growing season NDVI and the trends in T_{max} or T_{min}. R_P indicates partial correlation coefficients of the trend of the growing season NDVI with the trend in T_{max} (or T_{min}) through controlling T_{min} (or T_{max}). ***$P < 0.01$. Correlations with no asterisk are not significant ($P > 0.10$).

in WRF3.2. We also found that the ET trend of WRF3.2 in S2 differs considerably from the observed ET trend (Fig. S11), indicating that the temporal ET trend is not correctly reproduced in the WRF S2 simulations. In WRF3.2, the sensitivity of simulated ET to the NDVI depends on the land surface model used (28), suggesting the need to improve the model parameterizations considering the specific biophysical characteristics of TP grassland vegetation (29). Compared with regions in the same latitude band, the TP is characterized by a combination of high radiation and low temperatures, as well as by complex soil water variability (30); these properties are difficult to reproduce in a land-surface model. WRF3.2 may also have systematic biases in modeling other ET-relevant processes, such as radiative transfer, boundary-layer dynamics, and cloud physics. Future climate simulations of the TP thus require more observations to improve the parameterization and calibration of ET.

Given model imperfections in simulating ET over the TP, we used a sensitivity analysis based on intrinsic biophysical mechanisms to estimate how much daytime surface temperature (T_s) can change for an NDVI increase of 0.1. It is assumed that two adjacent blocks of grassland share the same background climate state and have no horizontal flow between them. The only difference is that one block has an NDVI value 0.1 greater than the other. This increase in the NDVI by 0.1 could enhance ET by ~0.5 $mm \cdot d^{-1}$ and decrease albedo by 0.01 (Figs. S9 and S10). In accordance with a study by Lee et al. (18), the resulting difference in T_s is estimated as −0.76 °C (*Sensitivity Analysis Based on Intrinsic Biophysical Mechanisms*), which is within the range statistically estimated from observations (Fig. S7). The change of T_s can be further divided into two components, a warming of 0.16 °C due to the decreased albedo and a cooling of 0.92 °C due to the increased ET for an NDVI difference of 0.1 between a pair of grasslands under the same background climate (*Sensitivity Analysis Based on Intrinsic Biophysical Mechanisms*).

In addition to ET and albedo, other factors, such as changes in large-scale circulation and stratospheric ozone depletion, could modify surface energy budgets and the spatial patterns of the trend of air temperature over the TP. Our statistical analysis also suggests that the negative spatial correlation between $T_{max,trend}$ and $NDVI_{trend}$ is unlikely to be caused by the changes in large-scale flows (*Impacts of Large-Scale Flows and Stratospheric Ozone Depletion* and Fig. S12). In addition, there is no evidence indicating that large-scale flows directly affect the spatial pattern of temperature trend within the TP (31). Stratospheric ozone depletion has been hypothesized to contribute a larger warming over the northern plateau during the past few decades (32) but cannot explain the negative $T_{max,trend}/NDVI_{trend}$ correlation (*Impacts of Large-Scale Flows and Stratospheric Ozone Depletion*). In addition, the insignificance of the $T_{min,trend}/NDVI_{trend}$ correlation could result from other factors because the nocturnal boundary layer is more sensitive to energy/turbulence changes (13).

Discussion

The TP has a cold climate and is covered by cold grasslands that are similar to the cold grasslands of dry-tundra regions of the Arctic. However, in contrast to the Arctic, where increasing vegetation activity is estimated to warm local climate by reducing albedo (14, 15), the climate feedback of increased vegetation activity appears to be negative in the TP, due to the dominance of ET-induced cooling over albedo-induced warming in case of an increase of vegetation greenness. We believe that the predominant role of ET cooling is caused by the much higher level of solar radiation (29) found at the relatively low latitude of the TP compared with the level of solar radiation in the high-latitude Arctic. The temperature is low on the TP, and the temperature when TP vegetation photosynthesis reaches its maximum is also correspondingly low (33) (Fig. S13); cool growing season temperatures over the TP are thus probably not a strong limitation on ET. Under the high radiation, increased vegetation needs to transpire more water, thus sustaining cooling feedbacks during the growing season. Hence, the findings from high latitudes cannot be simply transferred to the TP.

Accurate simulation of land-surface processes in the TP, such as ET and sensible heat flux into the atmosphere, is essential for characterizing the land/climate coupling that strongly affects the Asian monsoon (9). It has been projected that vegetation productivity across the TP will continue to be enhanced under future climate warming (5, 34). Unlike the Arctic ecosystem, evaporative cooling with water supplied by melting soil-ice may continue over this region.

We are aware that a statistical correlation, no matter how strong, does not imply causality. Also, data uncertainties and model deficiencies prevent us from reaching a quantitative conclusion on the magnitude of the evaporative cooling feedback induced by

increased vegetation activity over the TP. The differences in observed ET and residual atmospheric effects on the NDVI would result in the difference in the magnitude of ET sensitivity to the NDVI. For instance, the machine-learning algorithm (ET_J) used static climatic variables (25); the Priestley and Taylor equation-based ET_G (24) used satellite-observed precipitation that is reported biased over the TP (Fig. S6), which may lead to an unrealistic ET response to change in the NDVI; and the ET_M used biophysical parameters for certain biomes globally (23) that may not accurately account for the unique TP vegetation and environment. Empirical analyses of observational data cannot quantitatively separate the compound impacts of multiple factors on T_{max}, nor can they accurately determine the sensitivity of T_{max} to greening. Nevertheless, the significant correlations between $T_{max,trend}$ and $NDVI_{trend}$ and between $T_{max,trend}$ and ET_{trend}, as well as the enhancing effect of greening on ET, did suggest that greening could have a cooling effect.

Further attribution needs both observational and modeling studies on all relevant physical mechanisms, which is challenging due to the scarcity of adequate observations and credible models over the TP. Consequently, the magnitude of the vegetation/climate feedbacks estimated here is still largely uncertain, as demonstrated by the difference between observations and the WRF model estimates. These differences highlight the need for further constraining land surface biogeophysical, hydrological, and other processes in climate models. Unfortunately, in the TP, the in situ data needed to characterize these processes are scarce and incomplete. Collecting new data should be a high priority: Measurements of all radiation components, sensible and latent heat fluxes, and ground heat storage are needed across a representative transect over the TP. Such data will allow us to quantify the feedbacks between the vegetation conditions and the surface heat fluxes. They will also help modelers to have a more realistic parameterization of surface processes in climate models. Experiments with these improved models should then result in better understanding of the role of the TP in the global climate system.

Methods

NDVI Data. We used NDVI data derived from observations by three spaceborne sensors: the AVHRR onboard National Oceanic and Atmospheric Administration satellites (7, 9, 11, 14, 16–18), the MODIS onboard the National Aeronautics and Space Administration Earth Observing System's satellite Terra, and VEGETATION onboard the satellite SPOT. The AVHRR NDVI data covering the period 1982–2010 were produced at spatial and temporal resolutions of 8 km and 15 d by the Global Inventory Modeling and Mapping Studies group (35). The MODIS NDVI data for the period 2000–2010 are from Collection 5, MOD13A2, with a 16-d composite and 1-km spatial resolution. Unlike the AVHRR, the MODIS has onboard calibration and precise orbit control, higher radiometric precision, atmospheric and viewing geometry corrections with physics-based algorithms, and higher fidelity (36). The SPOT NDVI dataset for the period 2000–2010 was produced every 10 d at a spatial resolution of 1 km. Compared with the biweekly AVHRR and MODIS NDVIs, the temporal resolution of the SPOT NDVI is 10 d, which gives 36 composites for a 1-y cycle (37). Averages of monthly NDVI data during the growing season were used to infer vegetation growth.

Climate Data. Daily T_{max}, T_{min}, and T_{mean}, as well as daily precipitation, for the period 1982–2010 were recorded at 55 meteorological stations with no missing data. These data were provided by China Meteorological Data Sharing System (cdc.nmic.cn/home.do).

ET Data. ET was extracted from three ET datasets produced by using the MODIS satellite observations (ET_M), the Priestley and Taylor equation driven by satellite data (ET_G), and a machine-learning algorithm using flux-tower ET measurements (ET_J). The theoretical model based on the Penman–Monteith equation (38) is driven by MODIS data and daily meteorological data to produce global ET (ET_M) (23). The Priestley and Taylor equation is driven by a variety of satellite-sensor products to estimate daily transpiration globally at 0.25° × 0.25° (ET_G) (24). The machine-learning algorithm is first trained mainly by ET measurements at the observing flux-tower sites of FluxNet and is then driven by surface geophysical information from satellite remote sensing and meteorological data to produce global monthly ET at 0.5° × 0.5° (ET_J) (25).

WRF Model. We also used WRF3.2 (26) to investigate the feedback of vegetation growth change on daytime temperature during the growing season. The model domain covers the TP, having 90 × 60 grid points in each of the zonal and meridional directions, with a horizontal grid spacing of 50 km. There are 27 vertical layers between the model top at 70 hPa and the surface, and the time step of the model integration is 180 s. The R-2 reanalysis data (39) from the National Center for Environmental Prediction/DOE are used to obtain the initial and lateral boundary data. The monthly satellite-retrieved LAI (40) from the AVHRR NDVI was linearly interpolated to give daily values and used to prescribe the model's lower boundary every 24 h. The model physics include the Kain–Fritsch convective parameterization scheme (41, 42), the WRF single moment 3-class cloud microphysics scheme (43), the National Center for Atmospheric Research Community Atmosphere Model (CAM3) radiation scheme (44), the YonSei University planetary boundary layer scheme (45), and the Noah land surface model (27). The Noah model was initialized using the vegetation categories from the USGS 24-category, 30-s dataset and soil texture derived from the US Department of Agriculture's 16-category State Soil Geographic Database. The initial soil moisture state and lower soil boundary temperatures come from the reanalysis data. We used four soil layers in the Noah land surface model; the thicknesses of the layers from top to bottom are 0.1, 0.3, 0.6, and 1.0 m, with a total soil depth of 2 m.

Analyses. To quantify the feedback of vegetation growth change on temperature during the growing season (May–September), we performed a multiple linear regression analysis in which $T_{max,trend}$ (or $T_{min,trend}$) for each climate station was set as the dependent variable and $NDVI_{trend}$ and $T_{min,trend}$ (or $T_{max,trend}$) were set as independent variables. This procedure removes the confounding effect of the temperature correlation between daytime and nighttime, and defines the coefficient of $NDVI_{trend}$ as the net effect. The corresponding NDVI value for each meteorological station was derived by averaging the NDVI over a window of 3 × 3 AVHRR NDVI pixels (or equivalent areas of MODIS and SPOT NDVIs) with the data from the meteorological station in the central pixel.

We performed two simulations using the WRF model with the Noah land surface scheme: one without (S1) and one with (S2) forced day-to-day changes in the LAI derived from the AVHRR NDVI during the period 1982–2010 (40). The integration period was 5 mo (May to September), starting each May 1 for 29 y. In the S1 simulation, throughout the entire period 1982–2010, the vegetation was prescribed with the LAI of 1982, whereas in the S2 simulation, vegetation growth varied with the satellite-derived LAI data from 1982 to 2010. The net effect of interactions between vegetation growth and temperature on T_{max} was derived from a multiple linear spatial regression analysis in which the growing season T_{max} difference between the S2 and S1 simulations (ΔT_{max}) for each grid over the plateau was set as the dependent variable and ΔT_{min} and $\Delta NDVI$ were set as independent variables. The effect of ET on T_{max} (T_{min}) was investigated by using spatial partial correlation between ΔET and ΔT_{max} (ΔT_{min}) and setting ΔT_{min} (ΔT_{max}) as the controlling variable. The sensitivity of T_{max} (T_{min}) to the NDVI was determined using spatial regression in which ΔT_{max} (ΔT_{min}) was set as the dependent variable and $\Delta NDVI$ and ΔT_{min} (ΔT_{max}) were set as the independent variables. The effect of vegetation on ET was determined using the spatial regression between $\Delta NDVI$ and ΔET.

We also used a sensitivity analysis based on intrinsic biophysical mechanisms (18) to estimate how much T_s would change for an NDVI increase of 0.1. It is assumed that two adjacent blocks of grassland share the same background climate state and have no horizontal flow between them. The only difference is that one block has an NDVI value 0.1 greater than the other. The equations of the intrinsic biophysical mechanisms are then used to calculate the response of T_s to a difference in the NDVI, based on the observed ET and albedo response to the NDVI (*Sensitivity Analysis Based on Intrinsic Biophysical Mechanisms*).

ACKNOWLEDGMENTS. This study was funded by the Strategic Priority Research Program (B) of the Chinese Academy of Sciences (Grant XDB03030404), a National Basic Research Program of China (Grant 2013CB956303), a program of National Natural Science Foundation of China (Grant 41125004), and a grant from Youth Innovation Promotion Association of the Chinese Academy of Sciences (Grant 2015055).

1. Yao T, et al. (2012) Different glacier status with atmospheric circulations in Tibetan Plateau and surroundings. *Nat Clim Change* 2(9):663–667.
2. Hansen J, Ruedy R, Sato M, Lo K (2010) Global surface temperature change. *Rev Geophys*, 10.1029/2010RG000345.
3. Piao S, et al. (2012) Impacts of climate and CO_2 changes on the vegetation growth and carbon balance of Qinghai-Tibetan grasslands over the past five decades. *Glob Planet Change* 98–99:73–80.
4. Kato T, et al. (2006) Temperature and biomass influences on interannual changes in CO_2 exchange in an alpine meadow on the Qinghai-Tibetan Plateau. *Glob Change Biol* 12(7):1285–1298.
5. Tan K, et al. (2010) Application of the ORCHIDEE global vegetation model to evaluate biomass and soil carbon stocks of Qinghai-Tibetan grasslands. *Global Biogeochem Cycles* 24(1):GB1013.
6. Wang S, et al. (2012) Effects of warming and grazing on soil N availability, species composition, and ANPP in an alpine meadow. *Ecology* 93(11):2365–2376.
7. Chen H, et al. (2013) The impacts of climate change and human activities on biogeochemical cycles on the Qinghai-Tibetan Plateau. *Glob Change Biol* 19(10): 2940–2955.
8. Liu XD, Yin ZY, Shao XM, Qin NS (2006) Temporal trends and variability of daily maximum and minimum, extreme temperature events, and growing season length over the eastern and central Tibetan Plateau during 1961-2003. *J Geophys Res Atmos*, 10.1029/2005jd006915.
9. Wu GX, et al. (2012) Thermal controls on the Asian summer monsoon. *Sci Rep*, 10.1038/srep00404.
10. Collatz GJ, et al. (2000) A mechanism for the influence of vegetation on the response of the diurnal temperature range to changing climate. *Geophys Res Lett* 27(20): 3381–3384.
11. Chapin FS, Eugster W, McFadden JP, Lynch AH, Walker DA (2002) Summer differences among Arctic ecosystems in regional climate forcing. *J Clim* 13(12):2002–2010.
12. Field CB, Lobell DB, Peters HA, Chiariello NR (2007) Feedbacks of terrestrial ecosystems to climate change. *Annu Rev Environ Resour* 32:1–29.
13. Zhou L, Dickinson RE, Tian Y, Vose RS, Dai Y (2007) Impact of vegetation removal and soil aridation on diurnal temperature range in a semiarid region: Application to the Sahel. *Proc Natl Acad Sci USA* 104(46):17937–17942.
14. Pearson RG, et al. (2013) Shifts in Arctic vegetation and associated feedbacks under climate change. *Nat Clim Change* 3(7):673–677.
15. Chapin FS, 3rd, et al. (2005) Role of land-surface changes in arctic summer warming. *Science* 310(5748):657–660.
16. Bounoua L, et al. (2000) Sensitivity of climate to changes in NDVI. *J Clim* 13(13): 2277–2292.
17. Jeong SJ, Ho CH, Kim KY, Jeong JH (2009) Reduction of spring warming over East Asia associated with vegetation feedback. *Geophys Res Lett* 36:L18705.
18. Lee X, et al. (2011) Observed increase in local cooling effect of deforestation at higher latitudes. *Nature* 479(7373):384–387.
19. Loarie SR, Lobell DB, Asner GP, Mu QZ, Field CB (2011) Direct impacts on local climate of sugar-cane expansion in Brazil. *Nat Clim Change* 1(2):105–109.
20. Houspanossian J, Nosetto M, Jobbágy EG (2013) Radiation budget changes with dry forest clearing in temperate Argentina. *Glob Change Biol* 19(4):1211–1222.
21. Chen B, et al. (2014) The impact of climate change and anthropogenic activities on alpine grassland over the Qinghai-Tibet Plateau. *Agric For Meteorol* 189–190:11–18.
22. Shen M, et al. (2014) Increasing altitudinal gradient of spring vegetation phenology during the last decade on the Qinghai-Tibetan Plateau. *Agric For Meteorol* 189–190: 71–80.
23. Mu Q, Zhao M, Running SW (2011) Improvements to a MODIS global terrestrial evapotranspiration algorithm. *Remote Sens Environ* 115(8):1781–1800.
24. Miralles DG, et al. (2011) Global land-surface evaporation estimated from satellite-based observations. *Hydrology and Earth System Sciences* 15(2):453–469.
25. Jung M, et al. (2010) Recent decline in the global land evapotranspiration trend due to limited moisture supply. *Nature* 467(7318):951–954.
26. Skamarock WC, et al. (2008) *A Description of the Advanced Research WRF* (National Center for Atmospheric Research, Boulder, CO), Version 3.
27. Chen F, Dudhia J (2001) Coupling an advanced land surface-hydrology model with the Penn State-NCAR MM5 modeling system. Part I: Model implementation and sensitivity. *Monthly Weather Review* 129(4):569–585.
28. Strahler AH, et al. (1999) *MODIS BRDF/Albedo Product: Algorithm Theoretical Basis Document* (NASA, Greenbelt, MD), Version 5.0.
29. Zheng D, Zhang Q, Wu WS (2000) *Mountain Geoecology and Sustainable Development of the Tibetan Plateau* (Kluwer Academic, Dordrecht, The Netherlands).
30. Yang K, Chen YY, Qin J (2009) Some practical notes on the land surface modeling in the Tibetan Plateau. *Hydrology and Earth System Sciences* 13(5):687–701.
31. Yang K, et al. (2014) Recent climate changes over the Tibetan Plateau and their impacts on energy and water cycle: A review. *Glob Planet Change* 112:79–91.
32. Guo DL, Wang HJ (2012) The significant climate warming in the northern Tibetan Plateau and its possible causes. *Int J Climatol* 32(12):1775–1781.
33. Gao Y, et al. (2014) A MODIS-based photosynthetic capacity model to estimate gross primary production in Northern China and the Tibetan Plateau. *Remote Sens Environ* 148:108–118.
34. Su F, Duan X, Chen D, Hao Z, Cuo L (2013) Evaluation of the global climate models in the CMIP5 over the Tibetan Plateau. *J Clim* 26(10):3187–3208.
35. Tucker CJ, et al. (2005) An extended AVHRR 8-km NDVI dataset compatible with MODIS and SPOT vegetation NDVI data. *Int J Remote Sens* 26(20):4485–4498.
36. Huete A, et al. (2002) Overview of the radiometric and biophysical performance of the MODIS vegetation indices. *Remote Sens Environ* 83(1-2):195–213.
37. Maisongrande P, Duchemin B, Dedieu G (2004) VEGETATION/SPOT: An operational mission for the Earth monitoring; presentation of new standard products. *Int J Remote Sens* 25(1):9–14.
38. Monteith JL (1965) Evaporation and environment. *The State and Movement of Water in Living Organisms. Nineteenth Symposium of the Society of Experimental Biology* (Cambridge Univ Press, Cambridge, UK), pp 205–234.
39. Kanamitsu M, et al. (2002) NCEP-DOE AMIP-II reanalysis (R-2). *Bulletin of the American Meteorological Society* 83(11):1631–1643.
40. Zhu Z, et al. (2013) Global data sets of vegetation leaf area index (LAI)3g and fraction of photosynthetically active radiation (FPAR)3g derived from global inventory modeling and mapping studies (GIMMS) Normalized Difference Vegetation Index (NDVI3g) for the period 1981 to 2011. *Remote Sens* 5(2):927–948.
41. Kain JS (2004) The Kain-Fritsch convective parameterization: An update. *Journal of Applied Meteorology* 43(1):170–181.
42. Kain JS, Fritsch JM (1990) A one-dimensional entraining detraining plume model and its application in convective parameterization. *Journal of the Atmospheric Sciences* 47(23):2784–2802.
43. Hong SY, Dudhia J, Chen SH (2004) A revised approach to ice microphysical processes for the bulk parameterization of clouds and precipitation. *Monthly Weather Review* 132(1):103–120.
44. Collins WD, et al. (2004) *Description of the NCAR Community Atmosphere Model (CAM 3.0)* (National Center for Atmospheric Research, Boulder, CO).
45. Hong S-Y, Noh Y, Dudhia J (2006) A new vertical diffusion package with an explicit treatment of entrainment processes. *Monthly Weather Review* 134(9):2318–2341.
46. Yang K, Koike T, Yang DW (2003) Surface flux parameterization in the Tibetan Plateau. *Boundary Layer Meteorol* 106(2):245–262.
47. Yang K, et al. (2008) Turbulent flux transfer over bare-soil surfaces: Characteristics and parameterization. *Journal of Applied Meteorology and Climatology* 47(1): 276–290.
48. Tang W, Yang K, He J, Qin J (2010) Quality control and estimation of global solar radiation in China. *Solar Energy* 84(3):466–475.
49. Gu S, et al. (2008) Characterizing evapotranspiration over a meadow ecosystem on the Qinghai-Tibetan Plateau. *J Geophys Res Atmos*, 10.1029/2007JD009173.
50. Maussion F, et al. (2014) Precipitation seasonality and variability over the Tibetan Plateau as resolved by the high Asia reanalysis. *J Clim* 27(5):1910–1927.
51. Yin Z-Y, Zhang X, Liu X, Colella M, Chen X (2008) An assessment of the biases of satellite rainfall estimates over the Tibetan Plateau and correction methods based on topographic analysis. *Journal of Hydrometeorology* 9(3):301–326.
52. Yong B, et al. (2015) Global view of real-time TRMM Multi-satellite precipitation analysis: Implication to its successor Global Precipitation Measurement mission. *Bull Amer Meteor Soc* 96(2):283–296.
53. Cao R, Shen M, Chen J, Tang Y (2014) A simple method to simulate diurnal courses of PAR absorbed by grassy canopy. *Ecol Indic* 46:129–137.
54. Wang X, et al. (2011) Spring temperature change and its implication in the change of vegetation growth in North America from 1982 to 2006. *Proc Natl Acad Sci USA* 108(4):1240–1245.
55. Reichstein M, et al. (2005) On the separation of net ecosystem exchange into assimilation and ecosystem respiration: Review and improved algorithm. *Glob Change Biol* 11(9):1424–1439.